The Effect of Reduction on Rhenium(I) Complexes with Binaphthyridine and Biquinoline Ligands: A Spectroscopic and Computational Study

Sarah L. Howell, Sonya M. Scott, Amar H. Flood, and Keith C. Gordon*

MacDiarmid Institute for Advanced Materials and Nanotechnology, Department of Chemistry, University of Otago, Union Place, Dunedin, New Zealand

Received: January 12, 2005; In Final Form: March 2, 2005

A number of rhenium complexes with binaphthyridine and biquinoline ligands have been synthesized and studied. These are $[Re(L)(CO)_3Cl]$ where L = 3,3′-dimethylene-2,2′-bi-1,8-naphthyridine (dbn), 2,2′-bi-1,8-naphthyridine (bn), 3,3′-dimethylene-2,2′-biquinoline (dbq), and 3,3′-dimethyl-2,2′-biquinoline (diq). This series represents ligands in which the electronic properties and steric preferences are tuned. These complexes are modeled using density functional theory (DFT). An analysis of the resonance Raman spectra for these complexes, in concert with the vibrational assignments, reveals that the accepting molecular orbital (MO) in the metal-to-ligand charge transfer (MLCT) transition is the LUMO and causes bonding changes at the inter-ring section of the ligand. The electronic absorption spectroelectrochemistry for the reduced complexes of $[Re(dbn)(CO)_3Cl]$, $[Re(dbq)(CO)_3Cl]$, and $[Re(diq)(CO)_3Cl]$ suggest that the singly occupied MO is delocalized over the entire ligand structure despite the nonplanar nature of the diq ligand in $[Re(diq)(CO)_3Cl]$. The IR spectroelectrochemistry for $[Re(dbn)(CO)_3Cl]$, $[Re(dbq)(CO)_3Cl]$, and $[Re(bn)(CO)_3Cl]$ reveal that reduction lowers the CO ligand vibrational frequencies to a similar extent in all three complexes. The substitution of naphthyridine for quinoline has little effect on the nature of the singly occupied MO. These data are supported by DFT calculations on the reduced complexes, which reveal that the ligands are flattened out by reduction: This may explain the similarity in the properties of the reduced complexes.

I. Introduction

Complexes with polypyridine ligands based on binaphthyridine and biquinoline are of interest because of their electrochemical properties.[1−3] Copper(I) complexes with these ligands show a range of behaviors upon electrochemical reduction. For binaphthyridine ligands, which are reasonably flat, reduction leads to the formation of a radical anion species.[4,5] With binaphthyridine ligands, which are twisted, reduction leads to the appearance of spectral features consistent with electron localization on a single naphthyridine ring system.[6] With biquinoline ligands, reduction leads to decomplexation.[6,7] Investigations of ruthenium(II) complexes with such ligands show similar behavior with respect to electrochemical reduction. For complexes of the type $[Ru(L)(bpy)_2]^{2+}$ (where bpy = 2,2′-bipyridine and L = binaphthyridine-type ligand), reduction results in the formation of a radical anion of L. For homoleptic complexes of the type $[Ru(L)_3]^{2+}$, reduction does not show characteristic $L^{\bullet-}$ features, and it is possible that the reducing electron is delocalized over two of the bidentate ligands.[8]

The rhenium(I) center has advantages over the copper(I) and ruthenium(II) moieties for the following reasons: (1) It stabilizes the reduction potential of the ligand.[9] (2) The CO units indicate the nature of the bonding about the metal center. This is well-documented for such complexes in their excited-state behavior.[10−13] (3) There is no interference from spectator ligands in the interpretation of electronic absorption or Raman spectra.[14−16] (4) Structurally distorted complexes such as $[Re(diq)(CO)_3Cl]$ are stable.[9]

Complexes with the rhenium(I) moiety are also of interest, because they can act as photocatalysts for the conversion of $CO_2 \rightarrow CO$.[17] Ruthenium complexes with these ligands have been postulated as molecular machine building blocks.[18] A clear understanding of the structural changes that such complexes undergo is critical to their successful implementation in photocatalysis of molecular machine applications.

DFT methods with a variety of basis sets have proven effective in predicting some of the properties of complexes, such as geometry, electrochemical and spectral properties,[19] electronic spectra,[20−24] and vibrational spectra.[25−34] For example, Seiger et al.[35] have used DFT methods to predict a number of properties associated with cobalt complexes with NO, CO, and 1,4-diaza-1,3-butadiene (DAB) ligands, [(DAB)Co(NO)(CO)]. They were able to show that the DFT methods provided an accurate predictor of structure; in their study, the bond lengths were predicted to within 0.02 Å of the crystallographic data. Furthermore, time-dependent density functional theory (TD-DFT) allowed for a clearer assignment of the electronic absorption spectra with a deviation between calculated and experimental data of between 0.2 and 0.5 eV. Frequency calculations were performed on the complexes and their reduced species. For the NO and CO ligands, their vibrational bands were predicted to shift down in frequency by 140 and 103 cm^{-1}, respectively, upon reduction. In the experimental data, the observed shifts were 112 cm^{-1} for the NO ligand (from 1689 to 1577 cm^{-1}) and 74 cm^{-1} for the CO ligand (from 1942 to 1868 cm^{-1}). Sieger's work demonstrates that DFT methods may be used on both the parent and reduced complex species.

We have undertaken an investigation of binaphthyridine and biquinoline (biq) ligands with the $\{Re(CO)_3Cl\}$ moiety (Figure 1) in order to probe how the electronic and structural variation of ligands adjusts the interactions of the ligand with the metal center.

* Email address: kgordon@alkali.otago.ac.nz.

10.1021/jp0502252 CCC: $30.25
Published on Web 03/30/2005

In studying these complexes using DFT methods, we have attempted to address the following questions: (1) How well do the calculations model the observables of the complexes, that is, the structures as ascertained by X-ray crystallography and vibrational spectra? (2) Do the calculations offer insight into the electronic transitions of the complexes? (3) Can the calculations offer insight into the structural changes that occur when such complexes are reduced? The reduced species have significance with respect to photocatalytic activity.[17]

II. Experimental Section

Compound Synthesis. The ligands bn, dbn, and dbq were prepared as previously described.[36,37] The ligand diq was prepared following the synthetic procedure for the preparation of dbn.[38] A quantity (0.21 g, 1.8 mmol) of 3,4-hexanedione and 0.43 g (3.5 mmol) of 2-aminobenzaldehyde were refluxed together for 4 h under nitrogen. The product was recrystallized from ethyl acetate after the solvent had been removed. Anal. Calcd. for $C_{18}H_{14}N_4 \cdot 2CH_2Cl_2$: C, 58.18; H, 4.40; N, 6.17. Found: C, 58.59; H, 4.50; N, 6.56%. (Yield 36%.)

The rhenium(I) complexes were prepared following the procedure outlined by Moya et al.[9,39] The complexes were purified by recrystallization from dichoromethane.

[Re(biq)(CO)$_3$Cl]. Anal. Calcd. for $C_{21}H_{12}N_2O_3ClRe$: C, 44.8; H, 2.14; N, 4.98. Found: C, 44.7; H, 1.98; N, 4.94%. (Yield 69%.)

[Re(dbn)(CO)$_3$Cl]. Anal. Calcd. for $C_{21}H_{12}N_4O_3ClRe$: C, 42.75; H, 2.03; N, 9.50. Found: C, 42.63; H, 1.93; N, 9.52%. (Yield 54%.) MS: 590 ($Re(dbn)(CO)_3ClH^+$), 555 ($Re(dbn)(CO)_3^+$).

[Re(dbq)(CO)$_3$Cl]. Anal. Calcd. for $C_{23}H_{14}N_2O_3ClRe \cdot CH_2Cl_2$: C, 42.73; H, 2.41; N, 4.28. Found: C, 42.9; H, 2.09; N, 4.22%. (Yield 49%.) MS: 588 ($Re(dbq)(CO)_3ClH^+$), 553 ($Re(dbq)(CO)_3^+$).

[Re(bn)(CO)$_3$Cl]. Anal. Calcd. for $C_{19}H_{10}N_4O_3ClRe \cdot CH_2Cl_2$: C, 37.01; H, 1.86; N, 8.63. Found: C, 37.24; H. 1.77; N, 8.80%. (Yield 44%.) MS: 528 ($Re(bn)(CO)_3^+$).

[Re(diq)(CO)$_3$Cl]. Anal. Calcd. for $C_{21}H_{14}N_4O_3ClRe \cdot CH_2Cl_2$: C, 42.71; H, 2.67; N, 4.15. Found: C, 42.21; H, 2.39; N, 4.04%. (Yield 36%.) MS: 590 ($Re(diq)(CO)_3ClH^+$), 555 ($Re(diq)(CO)_3^+$).

Perdeuteration of biquinoline was achieved using a variation on the method of Junk et al.[40]

d_{12}-2,2′-Biquinoline (d_{12}-biq). Anal. Calcd. for $C_{18}D_{12}N_2$: C, 80.60; H, 8.96; N, 10.5. Found:[41] C, 80.4; H, 8.82; N, 10.6%. (Yield 77%.) MS (EI) *m*/*z* 268 (M^+). ^2H NMR (CH_2Cl_2) $\delta =$ 8.87 (s, 2d), 8.38 (s, 2d), 8.22 (s, 2d), 7.94 (s, 2d), 7.79 (s, 2d), and 7.61 (s, 2d).

[Re(d_{12}-biq)(CO)$_3$Cl]. Anal. Calcd. for $C_{21}D_{12}N_2O_3ClRe$: C, 43.94; H, 4.18; N, 4.88. Found: C, 44.2; H, 4.00; N, 4.92%. (Yield 69%.) MS: 539 ($Re(d_{12}\text{-biq})(CO)_3^+$).

Physical Measurements. Electronic absorption spectra were measured using a Perkin-Elmer λ-19 spectrometer. Electrochemical and spectroscopic measurements used solvents of spectroscopic grade. These were further purified by distillation and were stored over 5 Å molecular sieves. The supporting electrolytes used in the electrochemical measurements were tetrabutylammonium perchlorate (TBAP) and tetrabutylammonium hexafluorophosphate (TBAH). These were purified by repeated recrystallizations from ethanol/water for TBAP or ethyl acetate/ether for TBAH.[42]

Cyclic voltammograms (CVs) were obtained from argon-purged degassed solutions of compound (ca. 1 mM) with a 0.1 M concentration of TBAP or TBAH present. The electrochemical cell consisted of a 1.6 mm diameter platinum working electrode embedded in a Kel-F cylinder with a platinum auxiliary electrode and a saturated potassium chloride calomel reference electrode. The CV was calibrated against a ferrocene/ferrocenium couple. The potential of the cell was controlled by an EG&G PAR 273A potentiostat with model 270 software.

Fourier transform (FT)-IR spectra were collected using a Perkin-Elmer Spectrum BX FT-IR system on a solid-state sample (KBr disks) or solutions ($CDCl_3$) contained in a transmission cell (0.5 mm path length) with CaF_2 windows.

FT-Raman spectra were collected on powder samples using a Bruker IFS-55 interferometer with an FRA/106 S attachment. The excitation source was an Nd:YAG laser with an excitation wavelength of 1064 nm. A Ge diode (D424) operating at room temperature was used to detect Raman photons. All spectra were taken with a laser power of 80 mW at the sample and a resolution of 4 cm^{-1}. Spectra were obtained using 16−200 scans.

For the electronic absorption spectroelectrochemistry, spectra were acquired at a series of applied potentials stepping through the oxidation or reduction of interest. IR spectroelectrochemistry was accomplished using an IR optically transmissive thin-layer electrode (OTTLE) cell. IR spectroelectrochemistry was accomplished using an IROTTLE cell. The IROTTLE cell was developed from a modification of that reported by Hartl.[43] The cell was made from a standard IR transmission cell (Specac). The three-electrode system is composed of a platinum grid working electrode, a platinum auxiliary electrode, and a silver wire pseudo-reference electrode and is contained in the spacer. The spacer assembly was constructed by fusing the electrodes between sheets of polyethylene plastic. Each electrode was set across the entire width of the spacer to maintain equal stress across the NaCl windows when the whole cell is assembled. Each electrode grid had fused wire connectors protruding from the spacer assembly. These wire connectors were attached to the Teflon block assembly guide by copper screws. External wires were connected at the copper screws to provide connection to an external potentiostat.

A band-fitting analysis of the IROTTLE spectra was required because of incomplete electrochemical reduction. An analysis is necessary to quantify the IR band positions of the reduced state. The ground-state spectra were fitted to determine the positions, the bandwidths, and the relative intensities. These data were used as a starting point for fitting of the reduced spectra: the bands were centered with a ± 1.0 cm^{-1} variance, and heights were fixed relative to the band at ca. 2020 cm^{-1}. Widths of the lower two bands were constrained to reasonable estimates obtained from the ground-state bandwidths. The fitting was implemented with *GRAMS AI* software (Thermo Galactic) and used mixed Gaussian and Lorentzian band shapes.

A continuous-wave Innova I-302 krypton-ion laser (Coherent, Inc.) or MAP-543 argon-ion laser (Melles Griot) was used to generate resonance Raman (RR) scattering. Band-pass filters removed the Kr^+ plasma emission lines from the laser output. Typically, the laser output was adjusted to give 20 mW at the sample. The incident beam and the collection lens were arranged in a 135° backscattering geometry to reduce the attenuation of Raman intensity by self-absorption.[44] An aperture-matched lens was used to focus scattered light through a narrow band line-rejection (notch) filter (Kaiser Optical Systems) and a quartz wedge (Spex) and onto the 100 μm entrance slit of a spectrograph (Acton Research SpectraPro 500i). The collected light was dispersed in the horizontal plane by a 1200 grooves/mm ruled diffraction grating (blaze wavelength 500 nm) and detected

TABLE 1: Selected Bond Lengths for Calculated and Experimental Structures

	[Re(biq)-(CO)$_3$Cl] calcd	[W(biq)-(CO)$_4$] X-ray[a]	[Ru(biq)-(phen)$_2$]$^{2+}$ X-ray	[Re(dbq)-(CO)$_3$Cl] calcd	[Re(dbq)-(CO)$_3$Br] X-ray[c]	[Re(diq)-(CO)$_3$Cl] calcd	[Re(diq)-(CO)$_3$Br] X-ray[c]	[Re(dbn)-(CO)$_3$Cl] calcd	[Ru(bpy)$_2$-(dbn)]$^{2+}$ X-ray[d]	[Re(bn)-(CO)$_3$Cl] calcd	[Ru(bpy)$_2$–(bn)]$^{2+}$ X-ray[d]
r_1	1.481	1.494	1.478	1.474	1.474	1.492	1.495	1.468	1.475	1.475	1.469
r_2	1.418	1.416	1.419	1.423	1.448	1.434	1.423	1.426	1.413	1.421	1.400
r_3	1.341	1.321	1.355	1.340	1.375	1.339	1.345	1.340	1.344	1.342	1.346
r_4	1.378	1.404	1.382	1.377	1.365	1.371	1.376	1.375	1.387	1.377	1.377
r_5	1.432	1.403	1.439	1.432	1.406	1.429	1.400	1.428	1.418	1.437	1.406
r_6	1.418	1.419	1.412	1.418	1.394	1.418	1.403	1.349	1.358	1.350	1.347
r_7	1.378	1.384	1.371	1.378	1.367	1.377	1.373	1.318	1.332	1.318	1.321
r_8	1.415	1.416	1.416	1.415	1.384	1.417	1.385	1.417	1.406	1.416	1.405
r_9	1.376	1.325	1.359	1.375	1.381	1.376	1.345	1.375	1.351	1.375	1.344
r_{10}	1.418	1.439	1.435	1.419	1.419	1.419	1.430	1.417	1.413	1.416	1.415
r_{11}	1.414	1.390	1.407	1.413	1.430	1.412	1.403	1.414	1.411	1.415	1.393
r_{12}	1.370	1.367	1.343	1.374	1.347	1.380	1.357	1.373	1.352	1.369	1.354
r_{13}	1.081	0.959	0.950	1.508	1.477	1.514	1.506	1.509	1.503	1.082	0.959
r_{14}	2.235	2.279	2.088	2.239	2.203	2.285	2.218	2.215	2.086	2.213	2.103
r_{15}	1.928			1.928	1.914	1.915	1.900	1.933		1.933	
r_{16}	1.917			1.917	1.960	1.918	1.926	1.919		1.920	
r_{17}	1.159			1.159	1.136	1.162	1.165	1.158		1.158	
r_{18}	1.167			1.166	1.056	1.166	1.134	1.165		1.165	
r_{19}	1.081	0.997	0.950	1.512	1.505	1.513	1.502	1.512	1.520	1.082	0.960
r_{20}	1.928			1.926	1.948	1.921	1.911	1.932		1.933	
r_{21}	1.159			1.160	1.108	1.160	1.157	1.158		1.158	

[a] From ref 48. [b] From ref 18. [c] From ref 9. [d] From ref 5.

by a liquid-nitrogen-cooled back-illuminated Spec-10:100B charge coupled device (CCD) controlled by an ST-133 controller and *WinSpec/32* (version 2.5.8.1) software (Roper Scientific, Princeton Instruments).

The geometry and vibrational frequencies of the complexes were obtained using DFT-HF hybrid calculations implemented with the *Gaussian 03* program package.[45] The B3LYP calculations used an effective core potential (ECP) for rhenium (LANL2DZ basis set) and a 6-31G(d) basis set for all other atoms. Visualization of the MOs and vibrational modes was provided by the *Molden*[46] or *Molekel*[47] packages.

III. Results and Discussion

Geometry. The selected bond lengths for the calculated geometries for the complexes of interest are presented in Table 1. These may be compared to crystallographic data from the literature. In the case of [Re(biq)(CO)$_3$Cl], the related structures [W(biq)(CO)$_4$][48] and [Ru(phen)$_2$(biq)]$^{2+}$ [18] have been reported. The calculations show close agreement for the biq structure, with available crystallographic data. The mean absolute deviation for bond lengths on the ligand is 0.01 Å. The greatest disparity between experimental and calculated data is at the metal−nitrogen linkage. The ECP appears to be effective in modeling the interaction between the metal and ligand; there is a 0.04 Å deviation (for the metal−nitrogen linkage) between [W(biq)(CO)$_4$] and [Re(biq)(CO)$_3$Cl] and 0.147 Å for [Ru(phen)$_2$(biq)]$^{2+}$ and [Re(biq)(CO)$_3$Cl]. The metal−nitrogen bond length deviation between the calculated [Re(biq)(CO)$_3$Cl] and experimentally determined [Ru(phen)$_2$(biq)]$^{2+}$ structures is not surprising, because the [Re(biq)(CO)$_3$Cl] complex has significant CO back-bonding, which is absent in [Ru(phen)$_2$(biq)]$^{2+}$. In the case of [Re(dbq)(CO)$_3$Cl], crystallographic data on the bromide complex is available.[9] The mean absolute deviation for ligand bonds between calculated and experimental data in 0.005 Å. The only major bonding difference which occurs is for the axial CO (r_{18}) opposite the halogen atom. For the [Re(diq)(CO)$_3$Cl] complex, crystallographic data is available for the bromide.[9] The mean absolute deviation between the bond lengths observed in the crystallographic structure of [Re(diq)(CO)$_3$Br] and that calculated for [Re(diq)(CO)$_3$Cl] is 0.02 Å. The calculated structure of [Re(dbn)(CO)$_3$Cl] may be compared to the crystallographic structure [Ru(bpy)$_2$(dbn)]$^{2+}$:[5] in this case, the mean absolute deviation for the ligand bonds is 0.01 Å. As is the case for the [Re(biq)(CO)$_3$Cl] and [Ru(phen)$_2$(biq)]$^{2+}$ comparison, there is a 0.13 Å difference between the calculated Re−N and Ru−N bond lengths. For the bn complexes, comparison between calculated [Re(bn)(CO)$_3$Cl] and experimental [Ru(bpy)$_2$(bn)]$^{2+}$ [5] shows a mean absolute deviation for the ligand bonds of 0.01 Å. The metal−nitrogen linkage discrepancy is larger at 0.1 Å.

Having established the agreement between the calculated structures and crystallographic data, it is worth examining the structural differences that are predicted for the series of complexes. In all of the structures calculated, the Re(CO)$_3$Cl moiety sits above the ligand, which is generally bowed. Two substitution effects are of interest: (1) the torsion of the linked quinoline or naphthyridine rings as substitutions are made at Y or Z (Figure 1) and (2) the effect on the structure of substituting quinoline for naphthyridine rings. Substituents at the Y or Z positions primarily affect the dihedral angle between the ring systems: For [Re(biq)(CO)$_3$Cl], this is close to planar (177° for the dihedral angle described by r_3, r_1, r_2'); with [Re(dbq)(CO)$_3$Cl], it decreases to 172°; and finally, it decreases to 133° for [Re(diq)(CO)$_3$Cl]. The changes ongoing for biq to bn are very subtle; there are bond length and angle changes about the added N atoms, but the only other change is that the metal sits closer to the plane of the ligand (the dihedral angle defined by r_3, r_1, r_2' lowers from 22° for [Re(biq)(CO)$_3$Cl] to 14° for [Re(bn)(CO)$_3$Cl]).

Vibrational Spectra. *Carbonyl Region (1800−2100 cm^{-1}).* The IR spectral data for the carbonyl region are presented in Table 2. The pattern of bands is consistent with the adoption of a facial geometry for the three CO units about the rhenium(I) center.[11] The bands are assigned from highest to lowest wavenumber as a′(1), a″, and a′(2), respectively, according to recent computational and spectroscopic papers.[26−28,49,50] The vibrational analysis assigns the three carbonyl bands[26] going from highest to lowest frequency as $0.47r_{18} + 0.62r_{17} + 0.62r_{21}$ (Figure 1) which has a′ symmetry, designated a′(1), in the C_s point group, $0.88r_{18} - 0.33r_{17} - 0.33r_{21}$, designated a′(2), also

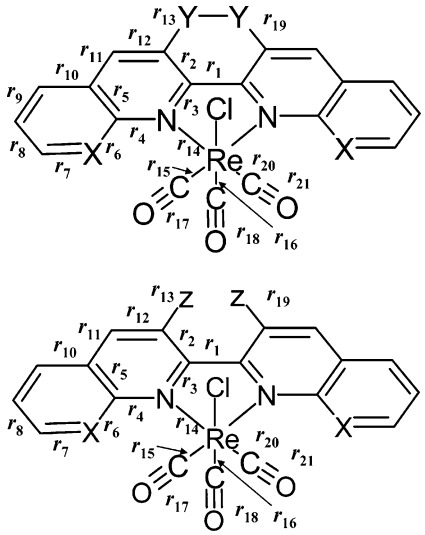

Figure 1. Structure and bond numbering system for [Re(L)(CO)$_3$Cl]. [Re(biq)(CO)$_3$Cl] X = CH, Z = H. [Re(dbq)(CO)$_3$Cl] X = CH, Y = CH$_2$. [Re(dbn)(CO)$_3$Cl] atom numbers X = N, Y = CH$_2$. [Re(diq)(CO)$_3$Cl] X = CH, Z = CH$_3$. [Re(bn)(CO)$_3$Cl] X = N, Y = H.

TABLE 2: IR Spectral Data, Experimental and Calculated for Complexes[a]

	ν/cm^{-1}				
complex	a′(1)[b]	a″[b]	a′(2)[b]	k_{av}/N m^{-1}	Δk_{av}/N m^{-1}
[Re(bpy)(CO)$_3$Cl][c]	2019	1917	1895	1527	44
[Re(bpy)(CO)$_3$Cl]$^-$ [c]	1996	1883	1868	1483	
[Re(abpy)(CO)$_3$Br][c]	2028	1943	1917	1556	58
[Re(abpy)(CO)$_3$Br]$^-$ [c]	2004	1900	1871	1498	
[Re(biq)(CO)$_3$Cl]	2016	1920	1898	1528	
	2104	*2036*	*2004*		
[Re(dbq)(CO)$_3$Cl]	2022	1920	1898	1531	49
	2105	*2035*	*2006*		
[Re(dbq)(CO)$_3$Cl]$^-$	1998	1882	1864	1482	
	2078	*1995*	*1972*		
[Re(dbn)(CO)$_3$Cl]	2017	1917	1887	1521	44
	2105	*2042*	*2011*		
[Re(dbn)(CO)$_3$Cl]$^-$	1997	1886	1852	1477	
	2073	*1993*	*1964*		
[Re(bn)(CO)$_3$Cl]	2016	1918	1887	1522	45
	2104	*2041*	*2012*		
[Re(bn)(CO)$_3$Cl]$^-$	1996	1884	1855	1477	
	2080	*2000*	*1973*		
[Re(4,4′bpy)$_2$(CO)$_3$Cl][d]	2026	1922	1895	1533	24
[Re(4,4′bpy)$_2$(CO)$_3$Cl]$^-$ [c]	2012	1903	1882	1509	
[Re(diq)(CO)$_3$Cl]	2020	1909	1892	1514	
	2105	*2026*	*2007*		

[a] Values predicted by DFT calculation (unscaled) are in italics. [b] Ref 49. [c] Ref 52. [d] Ref 10.

with a′ symmetry, and $0.71r_{17} - 0.71r_{21}$ with a″ symmetry, designated a″. The wavenumbers observed are slightly higher for the a′(1) and a′(2) vibrations in [Re(dbq)(CO)$_3$Cl] than for the [Re(dbn)(CO)$_3$Cl] complex. It is interesting to note that the force constants,[51,52] as calculated from the carbonyl band wavenumbers, are identical for [Re(diq)(CO)$_3$Cl] and [Re(dbq)(CO)$_3$Cl], despite the distortion of the diq ligand. This is also borne out in the work of Moya et al. on Br analogues of the diq and dbq complexes.[9] It suggests that the {Re(CO)$_3$Cl} moiety is enforcing significant structural requirements on the ligands rather than the other way around. Hence, it is the requirements of the metal moiety that dominate the structural nature of the complex. This is significant with respect to the comparison of dbn and dbq in the IR and electronic absorption spectroelectrochemistry. The frequency calculations on the complexes reveal that there are only small changes in the CO band frequencies going from dbn to dbq complexes as observed experimentally. For [Re(diq)(CO)$_3$Cl], the carbonyl bands lie at 2020, 1909, and 1892 cm^{-1}, and the unscaled frequencies are predicted at 2105, 2026, and 2007 cm^{-1}. These two sets of values are close to those observed and predicted for [Re(biq)(CO)$_3$Cl] and [Re(bn)(CO)$_3$Cl]. It is interesting to note that the a″ band which lies at 1909 cm^{-1} for [Re(diq)(CO)$_3$Cl] shifts to1920 cm^{-1} for [Re(biq)(CO)$_3$Cl] in the experimental data. This shift is predicted with bands at 2026 cm^{-1} in [Re(diq)(CO)$_3$Cl] and 2036 cm^{-1} in [Re(biq)(CO)$_3$Cl].

Polypyridyl Region (1000−1650 cm^{-1}). The IR spectra of these complexes are dominated by the carbonyl bands. The Raman spectra show strong bands in the 1000−1650 cm^{-1} region where the ligand modes are active with comparatively weak carbonyl bands. The data for the complexes [Re(biq)(CO)$_3$Cl] and [Re(d_{12}-biq)(CO)$_3$Cl] (its deuterated analogue) are shown in Figure 2. Analysis of the differences between experimental and calculated frequencies for bands that are medium-to-strong intensity (relative intensity > 0.1 relative to the strongest band in the region with relative intensity = 1) reveal that, with a scaling factor of 0.9729 *applied to all calculated data*, the mean absolute deviations are 7, 7, 6, and 5 cm^{-1} for [Re(biq)(CO)$_3$Cl], [Re(bn)(CO)$_3$Cl], [Re(dbn)(CO)$_3$Cl], and [Re(dbq)(CO)$_3$Cl], respectively. The general correspondence between the calculated and experimental relative intensities is also satisfactory.

A number of normal modes are common to the calculated Raman spectra of each of the complexes, which are also observed in the experimental data. For [Re(biq)(CO)$_3$Cl], the strong band predicted at 1604 cm^{-1} corresponds to $r_1 - r_{12} - r_{12'}$. This mode is also predicted to be present in [Re(dbq)(CO)$_3$Cl] at 1604 cm^{-1} and in [Re(dbn)(CO)$_3$Cl] and [Re(bn)(CO)$_3$Cl] at 1607 and 1599 cm^{-1}, respectively. The intense band predicted at 1470 cm^{-1} in [Re(biq)(CO)$_3$Cl] corresponds to $r_1 - r_3 - r_{3'} - r_6 - r_{6'}$ and is also predicted at 1463 cm^{-1} in [Re(dbq)(CO)$_3$Cl]. For [Re(bn)(CO)$_3$Cl] and [Re(dbn)(CO)$_3$Cl], the bands predicted at 1443 and 1449 cm^{-1}, respectively, correspond to $r_1 - r_3 - r_{3'}$. A similar normal mode is predicted at 1347, 1361, and 1335 cm^{-1} in [Re(biq)(CO)$_3$Cl], [Re(dbq)(CO)$_3$Cl], and [Re(bn)(CO)$_3$Cl], respectively. Frequency calculations on [Re(dbq)(CO)$_3$Cl] and [Re(dbn)(CO)$_3$Cl] show modes at 1431 and 1428 cm^{-1} that are described by $r_1 - r_2 - r_{2'}$. A mode described by $r_5 + r_{5'}$ is predicted at 1376, 1373, 1380, and 1379 cm^{-1} for [Re(biq)(CO)$_3$Cl], [Re(bn)(CO)$_3$Cl], [Re(dbn)(CO)$_3$Cl], and [Re(dbq)(CO)$_3$Cl], respectively.

A number of attempts to measure [Re(diq)(CO)$_3$Cl] Raman spectra were unsuccessful; however, the experimental IR spectral data may be compared to the calculated spectrum. The two spectra are shown in Figure 3. The mean absolute deviation between the calculated and experimental [Re(diq)(CO)$_3$Cl] IR spectra is 9 cm^{-1} for medium-to-strong bands in the 1000−1650 cm^{-1} region. The IR spectra of all the complexes are dominated by CO bands, and all of the other features are almost an order of magnitude less intense in the spectra.

Electronic Spectra. The electronic spectral data for the complexes are presented in Table 3. Each complex shows a lowest-energy transition, which is MLCT in nature.[2] The energy of the MLCT transition is related to the electrochemistry (Table 4) in that for ligands that are easy to reduce, such as bn and dbn, the MLCT transition is red-shifted with respect to those that are harder to reduce, including dbq and diq. This relationship has been well-documented for many polypyridyl complexes.[53−55] For the series of complexes studied herein, the reduction potential, which is related to the energy of the π^*

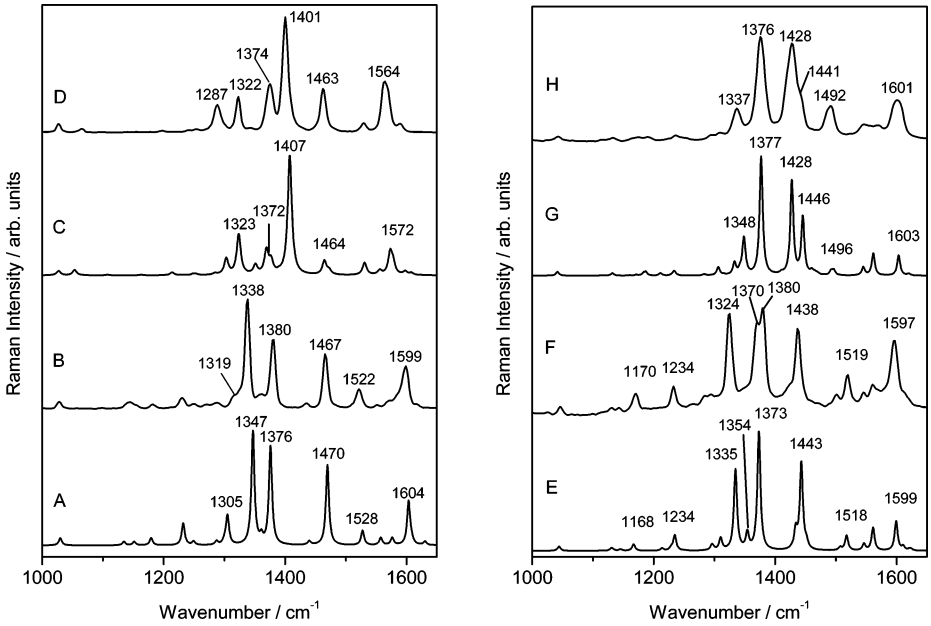

Figure 2. Calculated and experimental normal Raman spectra for (A) calculated Raman spectrum of [Re(biq)$(CO)_3$Cl]; (B) solid-state FT-Raman spectrum of [Re(biq)$(CO)_3$Cl]; (C) calculated spectrum of [Re(d_{12}-biq)$(CO)_3$Cl]; (D) solid-state FT-Raman spectrum of [Re(d_{12}-biq)$(CO)_3$Cl]; (E) calculated spectrum of [Re(bn)$(CO)_3$Cl]; (F) solid-state FT-Raman spectrum of [Re(bn)$(CO)_3$Cl]; (G) calculated spectrum of [Re(dbn)$(CO)_3$Cl]; (H) solid-state FT-Raman spectrum of [Re(dbn)$(CO)_3$Cl].

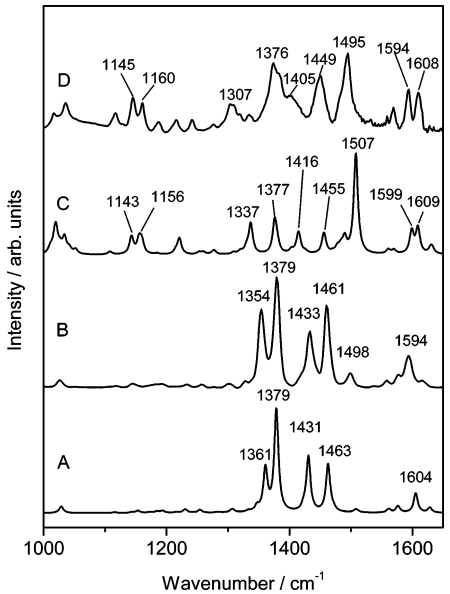

Figure 3. Calculated and experimental vibrational spectroscopic data for (A) calculated spectrum of [Re(dbq)$(CO)_3$Cl]; (B) solid-state FT-Raman spectrum of [Re(dbq)$(CO)_3$Cl]; (C) solid-state IR spectrum of [Re(diq)$(CO)_3$Cl]; (D) calculated IR spectrum of [Re(diq)$(CO)_3$Cl].

MO of the ligand, is tuned by 250 mV. This tuning is reflected in the UV−vis spectra where the MLCT band for [Re(dbn)$(CO)_3$Cl] lies at 499 nm (2.48 eV), whereas that for [Re(diq)$(CO)_3$Cl] is at 413 nm (3.00 eV). The results of TD-DFT calculations for the complexes of interest are summarized in Table 3, including the configurations for each predicted transition. These data are compared to the experimental spectral data (also shown in Table 3). The values for the MLCT transition energies are underestimated by 0.3−0.7 eV. However, the shifts in MLCT energy going across the series are reproduced well. For example, strong MLCT transitions are predicted for [Re(bn)$(CO)_3$Cl] and [Re(dbn)$(CO)_3$Cl] at about 700 nm (1.77 eV), whereas these transitions in [Re(dbq)$(CO)_3$Cl] are predicted at 623 nm (1.99 eV) and in [Re(diq)$(CO)_3$Cl] at 534 nm (2.32 eV). In each of these cases, the principal configuration is HOMO − 1 → LUMO. Although the absolute values are incorrect, the direction of the spectral shifts is correctly predicted along with the magnitude of the shifts. In a detailed study of the electronic spectral properties of [$W(CO)_4$(1,2-ethylenediamine)] and related compounds, Zális et al. also found that the calculated transition energies showed a 0.3−0.6 eV discrepancy from experimental results, although trends with substitution were evident.[56] Furthermore, the higher-lying unoccupied MOs such as LUMO + 1 and LUMO + 2 are not predicted to be involved in any of the lower-lying transitions.

Resonance Raman Spectra. The resonance Raman phenomenon may be used to probe the nature of chromophore transitions.[57] Such experiments have been applied to metal complexes to identify the nature of absorbing chromophores.[58−60] Indeed, it is possible to analyze the Raman band enhancements pattern as a function of excitation wavelength (an excitation profile) to derive structural distortions going from the ground state to the resonant excited state.[61−63] Although we have not attempted to construct such a profile, we can use the resonance Raman data for [Re(biq)$(CO)_3$Cl] and its deuterated analogue, in comparison with the nonresonant spectra, to establish a qualitative understanding of the nature of the excited state, particularly with regard to the ligand.

The resonance Raman spectra for [Re(biq)$(CO)_3$Cl] (Figure 4) show strong enhancements of a carbonyl mode at 2022 cm^{-1} (not shown) and some ligand modes in the 1200−1600 cm^{-1} region. The strong enhancement of the a′(1) carbonyl mode is consistent with the MLCT assignment for the excitation wavelength used (457.9 nm).[64,65] The resonance enhancement is derived through A-term scattering;[61] thus, both of the totally symmetric modes, a′(1) and a′(2), may be enhanced. The preferential enhancement of the higher-frequency mode is a consequence of the normal mode of a′(1), which involves a distortion of the {$Re(CO)_3$} moiety which matches the photoexcitation of the MLCT excited state more effectively than that of a′(2). This has been illustrated in a paper by Morrison et al.[50] The ligand-based modes that are strongly enhanced in the resonance Raman spectra (457.9 nm) lie at 1467 and 1338 cm^{-1}.

TABLE 3: Calculated and Experimentally Observed Electronic Transitions for Complexes of Interest[a]

λ/nm	f	λ/nm (ϵ/mM^{-1} cm^{-1})	MO configuration (coefficients)
		[Re(biq)(CO)$_3$Cl] HOMO = MO 104	
659	0.002		104,105 (0.70)
570	0.033	441 (4)	102,105 (0.11) 103,105 (0.67)
481	0.012		102,105 (0.69)
408	0.001		100,105 (0.38) 104,106 (0.58)
408	0.009		98,105 (0.13) 99,105 (0.14) 101,105 (0.66)
396	0.045	374 (33)	100,105 (0.55) 104,106 (−0.39)
389	0.018	356 (12)	103,106 (0.69)
363	0.000		104,107 (0.70)
348	0.001		103,107 (0.70)
346	0.001		98,105 (0.66) 99,105 (0.12) 101,105 (−0.13)
337	0.001		97,105 (0.68)
		[Re(dbq)(CO)$_3$Cl] HOMO = MO 111	
733	0.000		111,112 (0.70)
623	0.032	434 (4)	109,112 (0.12) 110,112 (0.67)
515	0.012		107,112 (−0.12) 109,112 (0.68)
449	0.022	390 (21)	105,112 (0.21) 108,112 (0.65)
435	0.039		107,112 (0.65) 111,113 (0.13)
396	0.017	372 (13)	111,113 (0.69)
385	0.022		106,112 (−0.40) 110,113 (0.57)
382	0.030		105,112 (0.47) 106,112 (−0.38) 110,113 (−0.30)
		[Re(diq)(CO)$_3$Cl] HOMO = MO 112	
590	0.002		112,113 (0.70)
534	0.027	413 (5)	111,113 (0.68)
445	0.001		110,113 (−0.40) 112,114 (0.57)
436	0.018		110,113 (0.56) 112,114 (0.40)
422	0.024	359 (16)	111,114 (0.69)
382	0.038		106,113 (0.11) 109,113 (0.66)
367	0.010	322 (17)	106,113 (0.17) 108,113 (0.66)
353	0.015		110,114 (0.69)
346	0.003		107,113 (−0.23) 112,115 (0.66)
		[Re(bn)(CO)$_3$Cl] HOMO = MO 104	
968	0.001		104,105 (0.70)
721	0.023	499 (2)	102,105 (−0.34) 103,105 (0.58)
674	0.018		102,105 (0.61) 103,105 (0.29)
522	0.005		100,105 (−0.11) 104,106 (0.69)
480	0.038	393 (17)	103,106 (0.70)
470	0.000		101,105 (0.70)
448	0.042	372 (16)	100,105 (0.67)
441	0.002		104,107 (0.70)
		[Re(dbn)(CO)$_3$Cl] HOMO = MO 111	
954	0.001		111,112 (0.70)
719	0.027	499 (2)	109,112 (−0.31) 110,112 (0.59)
670	0.017		109,112 (0.63) 110,112 (0.26)
511	0.004		111,113 (0.69)
472	0.032	393 (17)	110,113 (0.70)
468	0.001		107,112 (−0.30) 108,112 (0.63)
447	0.044	372 (16)	107,112 (0.61) 108,112 (0.27)

[a] Measurements were made on complexes in CH_2Cl_2 solution at room temperature, calculations are in vacuo.

TABLE 4: Electrochemical Data for Complexes in CH_2Cl_2 at 298 K[a,b]

complex	E°/V reduction	
Re(dbn)(CO)$_3$Cl	−0.85	−1.47
Re(dbq)(CO)$_3$Cl	−1.03	−1.62 (i)[c]
Re(bn)(CO)$_3$Cl	−0.94	−1.57
Re(diq)(CO)$_3$Cl	−1.10	−1.65 (i)

[a] Potentials versus SCE ± 0.02 V. [b] Supporting electrolyte is 0.1 M TBAP. [c] (i) = irreversible process.

These modes do not involve vibrational motion at the r_{12} bond of the biq ligand. Modes that do have r_{12} character, such as 1599 and 1380 cm^{-1}, are not strongly enhanced in the resonance Raman spectrum. The calculated MOs show that the population of the LUMO (MO 105) for [Re(biq)(CO)$_3$Cl] has virtually no effect on the bonding of r_{12}. The donor orbitals in MLCT transitions are metal-based and have little effect on the structure of the ligand with depopulation;[66] in such transitions, the resonance Raman enhancement pattern of the ligand vibrations

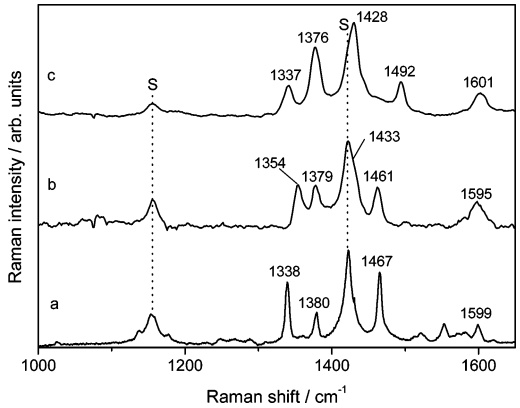

Figure 4. Resonance Raman spectra of (a) [Re(biq)(CO)$_3$Cl], 3 mM CH_2Cl_2 solution, 457.9 nm excitation; (b) [Re(dbq)(CO)$_3$Cl], 1 mM CH_2Cl_2 solution, 413 nm excitation; (c) [Re(dbn)(CO)$_3$Cl], 3 mM CH_2Cl_2 solution, 413 nm excitation. S denotes solvent.

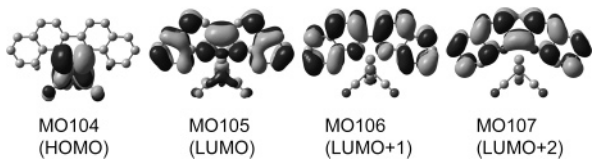

Figure 5. Depiction of molecular orbitals for [Re(biq)(CO)$_3$Cl].

reflects the acceptor orbital. Furthermore, population of the higher UMOs, such as LUMO + 1 and LUMO + 2 (Figure 5), would result in bonding changes at r_{12}. The pattern of enhancements is thus consistent with the population of the LUMO by the MLCT transition resonant at 457.9 nm. This is also consistent with the TD-DFT calculations, which show that the lowest transitions of appreciable intensity terminate on the LUMO for [Re(biq)(CO)$_3$Cl].

Resonance Raman spectra from [Re(dbn)(CO)$_3$Cl] and [Re(dbq)(CO)$_3$Cl] has been measured, but because of the strong emission from these samples, spectra were collected with 413 or 406 nm excitation. Furthermore, the strong emission signals swamped the CO region of the spectra. In both cases, the resonance Raman spectra show only very slight differences from the corresponding FT-Raman data. For [Re(dbn)(CO)$_3$Cl], the 1337 and 1492 cm^{-1} bands appear to have stronger relative intensities than other features. Both of these modes may be assigned to ligand stretches that contain significant inter-ring stretch character. For [Re(dbq)(CO)$_3$Cl], the relative intensities of the bands are very similar to the nonresonance spectrum. In the normal modes of this complex, all of the modes observed in the nonresonance and resonance Raman spectra have inter-ring stretch character.

The resonance Raman spectra suggest that the MLCT transitions in these complexes terminate on a ligand π^* MO in which the bonding at the inter-ring is altered. Interestingly, the changes in substituents have little effect on the electronic structural changes with excitation, although they do, of course, alter the energies of the transitions.

Spectroelectrochemistry. *Electronic Spectra.* The electrochemical data of the complexes is presented in Table 4. The electrochemical reduction of these complexes results in significant electronic spectral changes. These are summarized in Table 5. Absorptions are observed in the far-red region of the spectrum, but there is no obvious pattern based on the substituents evident in the spectra of the parent compounds. A number of studies have measured the spectra of reduced complexes containing binaphthyridine-type ligands. Spectroelectrochemical studies of copper(I) complexes with the dbn

TABLE 5: Electronic Absorption Data for Reduced Complexes in CH_2Cl_2 Solution at Room Temperature

complex	λ/nm (ϵ /10^3 M^{-1} cm^{-1})							
$[Re(dbn)(CO)_3Cl]^-$	364(17)	393(13)	413(10)	491(5)			796(2)	905(4)
$[Re(dbq)(CO)_3Cl]^-$	373(21)	391(25)	481(5)				809(2)	921(4)
$[Re(diq)(CO)_3Cl]^-$	352(18)	409(10)	473(5)	506(4)	614(2)	668(2)	734(2)	929(3)

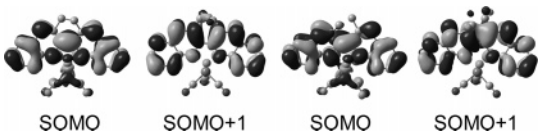

Figure 6. Molecular orbital depictions for the singly occupied MO (SOMO) and SOMO + 1 for $[Re(dbq)(CO)_3Cl]^{\bullet-}$, left-hand pair, and $[Re(diq)(CO)_3Cl]^{\bullet-}$, right-hand pair.

ligand show that the reduced species absorbs in the 900−1000 nm region. This was demonstrated to be due to the $dbn^{\bullet-}$ radical anion by analysis of the resonance Raman spectra of reduced ligands and complexes.[4,6] Copper(I) complexes reveal that the reduction shows a band at 900−1200 nm.[4,6] Those with the more sterically constrained tbn ligand (the ligand has a seven-membered central ring, Figure 1: Y−Y = $-(CH_2)_3-$) show strong absorbances at 700 nm. The latter is consistent with a radical anion that is naphthyridine in nature. The spectroelectrochemistry of ruthenium(II) complexes with dbn ligands shows that the first reduction of $[Ru(dbn)(bpy)_2]^{2+}$ shows a $dbn^{\bullet-}$ spectral signature, whereas the second reduction shows features similar to $naphthyridine^{\bullet-}$.[5,67] The spectral features observed for $dbn^{\bullet-}$ in the spectrum of $[Ru(dbn)(bpy)_2]^+$ lie at 900 nm. This would suggest that the reducing electron in $[Re(dbn)(CO)_3Cl]^-$ is delocalized over the dbn ligand in a fashion similar to that for $[Ru(dbn)(bpy)_2]^+$. The spectra of $[Re(dbq)(CO)_3Cl]^-$ and $[Re(diq)(CO)_3Cl]^-$ suggest that the reducing electron occupies a molecular orbital extended across the two fused ring systems. The electronic absorption spectrum of the quinoline radical anion lies at ca. 710 nm.[68] The transitions observed in the spectra of the reduced complexes are shifted significantly to the red of this, suggesting a greater delocalization of the electron across the two π ring systems in $[Re(dbn)(CO)_3Cl]$, $[Re(dbq)(CO)_3Cl]$, and $[Re(diq)(CO)_3Cl]$. This is consistent with the MOs generated for the calculations of the reduced complexes, which show the $[Re(diq)(CO)_3Cl]$ to have a delocalized nature in the singly occupied MO (SOMO) and SOMO + 1, very similar to that for $[Re(dbn)(CO)_3Cl]$ or $[Re(dbq)(CO)_3Cl]$, which both possess much flatter ligands in the reduced complexes (Figure 6).

Vibrational Spectra. Attempts to generate resonance Raman spectra from reduced complexes were unsuccessful because of excessive emission from the samples of interest. However, the nature of the metal-to-ligand interaction may be probed through IR spectroelectrochemistry. This is well-suited to probing the CO bands but is mute to the ligand vibrations due to the interference of the solvent and electrolyte IR absorption spectra. The data for these compounds and their reduced species are presented in Table 2. The greater the overlap between the MOs is, the larger the extent of charge leakage is from the π^* to $d\pi$ MOs when the complex is reduced.[14,26,28,69] As the $d\pi$ MOs are overlapped with the π^* MOs of the CO ligands, this charge leakage results in a decrease in bond order of the CO ligands and a corresponding wavenumber lowering for the CO bands. The CO ligands are therefore acting as electron density sensors of the metal site. The dbn and dbq complexes offer an interesting contrast, because they are structurally similar yet have different electronic properties. The IR spectroelectrochemistry for the dbn and dbq complexes show that the wavenumbers of the CO stretches are shifted to lower values with reduction at the ligand.

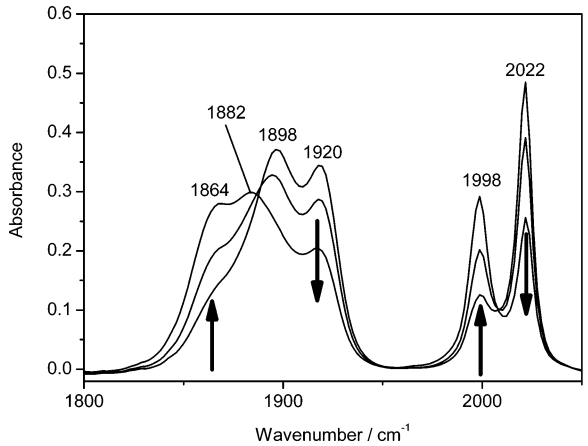

Figure 7. IR spectra of $[Re(dbn)(CO)_3Cl]$ (5 mM CH_2Cl_2 solution) undergoing reduction in the IROTTLE cell. Spectral changes are indicated by arrows.

The magnitude of these shifts may be related to changes in the CO ligand bond orders by the change in the average force constant, Δk_{av}, as described by Stor et al.[52,70,71] The results from this study and a number of previously reported findings are presented in Table 2. An example of the spectra generated in the IROTTLE experiment is shown in Figure 7.

Complexes with azo-2,2′-bipyridine (abpy) and 4,4′-bipyridine (4,4′-bpy) are included, because they represent extremes of behavior with respect to metal $d\pi$−ligand π^* overlap. The π^* MO of the 4,4′-bpy ligand is characterized by low overlap with the metal $d\pi$, and consistent with this, the Δk_{av} value is 24 N m^{-1}. This is also the case for the related $[Re((CO_2)_2\text{-bpy})(MQ^{\bullet/+})(CO)_3Cl]^{+/0}$ in which the reducing electron resides on the $MQ^{\bullet}$ moiety.[72] Both of these complexes show much smaller Δk_{av} values than those observed for $[Re(bpy)(CO)_3Cl]^{0/-}$. The data for $[Re(abpy)(CO)_3Br]^{0/-}$ shows Δk_{av} of 58 N m^{-1}, which is higher than that for the bpy complex and the complexes reported herein. The abpy ligand belongs to an important class of polypyridyl ligands with very low π^* MO energies and large wave function amplitudes at the chelating N for π^*. This has been demonstrated experimentally, through spectroelectrochemical EPR, and has been supported by quantum calculations.[73]

The Δk_{av} values for the complexes reported herein are the same, within experimental error. This suggests that the ligand−metal overlap is unchanged when increasing the heteroatom content of the ligand dbq → dbn. It is also interesting to note that the Δk_{av} values are similar to those observed for bpy complexes. Furthermore, DFT calculations on the reduced complexes provide frequency data which may be compared to that experimentally obtained. The unscaled frequencies of the CO bands in the parent and reduced complexes are presented in Table 2. The calculated bands overestimate the observed frequencies; however, the predicted bands clearly show that substitution of the ligand has little effect on the CO bands and reduction lowers the band frequencies equally for all three complexes for which there is data. Thus, the calculations accurately predict the electronic changes in the complexes with reduction.

TABLE 6: Selected Bond Lengths for Calculated Structures of Reduced Complexes

	$[Re(biq)(CO)_3Cl]^{\bullet-}$	$[Re(dbn)(CO)_3Cl]^{\bullet-}$	$[Re(bn)(CO)_3Cl]^{\bullet-}$	$[Re(dbq)(CO)_3Cl]^{\bullet-}$	$[Re(diq)(CO)_3Cl]^{\bullet-}$
r_1	1.437	1.433	1.437	1.431	1.442
r_2	1.426	1.433	1.426	1.432	1.441
r_3	1.372	1.367	1.369	1.370	1.377
r_4	1.379	1.368	1.369	1.378	1.371
r_5	1.434	1.437	1.436	1.435	1.432
r_6	1.418	1.352	1.351	1.417	1.418
r_7	1.388	1.328	1.326	1.388	1.385
r_8	1.407	1.405	1.403	1.407	1.407
r_9	1.389	1.391	1.389	1.389	1.387
r_{10}	1.410	1.405	1.403	1.411	1.409
r_{11}	1.431	1.428	1.427	1.430	1.428
r_{12}	1.366	1.369	1.364	1.368	1.371
r_{13}	1.083	1.512	1.083	1.513	1.517
r_{14}	2.231	2.237	2.230	2.238	2.212
r_{15}	1.925	1.925	1.924	1.925	1.922
r_{16}	1.906	1.904	1.905	1.907	1.905
r_{17}	1.166	1.166	1.165	1.167	1.165
r_{18}	1.173	1.173	1.172	1.173	1.172
r_{19}	1.083	1.509	1.083	1.509	1.518
r_{20}	1.925	1.924	1.924	1.924	1.925
r_{21}	1.166	1.166	1.165	1.166	1.166

Geometries of reduced complexes. The calculated geometries for the reduced complexes are presented in Table 6. These were established by using unrestricted B3LYP calculations with an extra electron added to the structure. These show that the major structural changes in bond lengths occur at r_1 and r_2, with the former shortening between 0.035 and 0.050 Å and the latter lengthening. The reduced complexes $[Re(dbn)(CO)_3Cl]$, $[Re(bn)(CO)_3Cl]$, and $[Re(diq)(CO)_3Cl]$ also show major bond length changes at $r_{14'}$, the metal chelate linkage. There are also a number of more subtle bonding changes; in all cases, the ligand flattens out with reduction. For example, in the case of $[Re(diq)(CO)_3Cl]$, the dihedral angle defined by r_3, r_1, and $r_{3'}$ alters from $-37.7°$ to $-24.3°$. Finally, the carbonyl bonds are lengthened in all cases with reduction, consistent with the observation of reduced vibrational frequencies in the IROTTLE experiments. These calculated changes are similar across the series of compounds, which is consistent with the very similar results, in terms of frequency shifts of the carbonyl bands, observed in the OTTLE experiments.

IV. Conclusions

A number of conclusions may be drawn from this study. In the first instance, it is clear that the B3LYP method in conjunction with the appropriate ECP, in this case LANL2DZ, and the 6-31G(d) basis set on the other atoms models the structures of these complexes with good accuracy. The deviation between experimental and calculated ligand bond lengths is <0.02 Å. Importantly, the calculations also correctly predict structural changes that occur with substitution. For example, the inter-ring bond (r_1) is shortened going from $[Re(biq)(CO)_3Cl]$ to $[Re(dbq)(CO)_3Cl]$ but lengthened going to $[Re(diq)(CO)_3Cl]$. These changes are correctly predicted by calculation. The calculations are also effective in predicting the vibrational spectra of the ground states of the respective complexes; both frequencies and intensities in IR and Raman spectra are predicted. The frequencies show a mean absolute deviation of <10 cm^{-1} for the polypyridyl region. Again, the calculations are particularly effective in predicting substitution effects; this is exemplified by the Raman spectra of $[Re(biq)(CO)_3Cl]$ and $[Re(bn)(CO)_3Cl]$ compared to $[Re(dbn)(CO)_3Cl]$ and $[Re(dbq)(CO)_3Cl]$. For the unbridged ligands, the pattern of bands shows three strong features at 1338, 1380, and 1467 cm^{-1} in $[Re(biq)(CO)_3Cl]$ and 1324, 1380, and 1438 cm^{-1} in $[Re(bn)(CO)_3Cl]$. The complexes with ligands with a central six-membered ring have an additional feature at 1428 cm^{-1} for $[Re(dbn)(CO)_3Cl]$ and 1433 cm^{-1} for $[Re(dbq)(CO)_3Cl]$, which is predicted. Furthermore, the shifts of the existing bands are also predicted.

Time-dependent DFT methods have proven useful in ascertaining the nature of the MLCT transition. A number of transitions for each complex are present in the visible region: all of these terminate on the LUMO, which is a π^* MO of the ligand. An analysis of the resonance enhancement patterns shows that modes that are associated with r_{12} and $r_{12'}$ bonds are not enhanced. This is consistent with the population of the LUMO, which does not affect the bonding in this region: the higher-lying UMOs do have an effect on the r_{12} and $r_{12'}$ linkages. It is also interesting to note that the TD-DFT calculations are able to predict the effects on electronic transitions of substitution, although the absolute values are generally too high in energy.

Finally, the spectroelectrochemistry reveals that the rhenium(I) complexes differ somewhat from complexes with these ligands with copper(I) or ruthenium(II). The electronic absorption spectra of the reduced complexes point to an SOMO that is delocalized across the ligand structure for dbn, dbq, and diq, and this is consistent with the calcautions on the reduced species. The calculations on the reduced complexes suggest that substitution has very little effect on the nature of the accepting MO in the reduced compound (i.e., it is a π^* ligand MO). This is substantiated in the IR spectroelectrochemistry, which shows that the changes in the average force constant for the CO ligands with reduction is virtually invariant with substitutional changes.

Acknowledgment. Support from the Foundation for Research, Science & Technology, the MacDiarmid Institute for Advanced Materials and Nanotechnology and the University of Otago is gratefully acknowledged.

References and Notes

(1) Von Zelewsky, A.; Gremaud, G. *Helv. Chim. Acta* **1988**, *71*, 1108.

(2) Moya, S. A.; Schmidt, R.; Pastene, R.; Sartori, R.; Mueller, U.; Frenzen, G. *Organometallics* **1996**, *15*, 3463.

(3) Thummel, R. P.; Lefoulon, F. *Inorg. Chem.* **1987**, *26*, 675.

(4) Scott, S. M.; Gordon, K. C.; Burrell, A. K. *Inorg. Chem.* **1996**, *35*, 2452.

(5) Scott, S. M.; Burrell, A. K.; Cocks, P. A.; Gordon, K. C. *J. Chem. Soc., Dalton Trans.* **1998**, 3679.

(6) Scott, S. M.; Gordon, K. C.; Burrell, A. K. *J. Chem. Soc., Dalton Trans.* **1998**, 2873.
(7) Page, S. E.; Gordon, K. C.; Burrell, A. K. *Inorg. Chem.* **1998**, *37*, 4452.
(8) Pérez-Cordero, E.; Brady, N.; Echegoyen, L.; Thummel, R.; Hung, C.-Y.; Bott, A. S. G. *Chem.—Eur. J.* **1996**, *2*, 781.
(9) Moya, S. A.; Guerrero, J.; Pastene, R.; Sartori, R.; Schmidt, R.; Sariego, R.; Sanz-Aparicio, J.; Fonseca, I.; Martinez-Ripoll, M. *Inorg. Chem.* **1994**, *33*, 2341.
(10) George, M. W.; Johnson, F. P. A.; Westwell, J. R.; Hodges, P. M.; Turner, J. J. *J. Chem. Soc., Dalton Trans.* **1993**, 2977.
(11) Gamelin, D. R.; George, M. W.; Glyn, P.; Grevels, F.-W.; Johnson, F. P. A.; Klotzbuecher, W.; Morrison, S. L.; Russell, G.; Schaffner, K.; Turner, J. J. *Inorg. Chem.* **1994**, *33*, 3246.
(12) George, M. W.; Johnson, F. P. A.; Turner, J. J.; Westwell, J. R. *J. Chem. Soc., Dalton Trans.* **1995**, 2711.
(13) Clark, I. P.; George, M. W.; Turner, J. J. *J. Phys. Chem. A* **1997**, *101*, 8367.
(14) Schoonover, J. R.; Strouse, G. F.; Chen, P.; Bates, W. D.; Meyer, T. J. *Inorg. Chem.* **1993**, *32*, 2618.
(15) Schoonover, J. R.; Strouse, G. F.; Omberg, K. M.; Dyer, R. B. *Comments Inorg. Chem.* **1996**, *18*, 165.
(16) Schoonover, J. R.; Strouse, G. F.; Dyer, R. B.; Bates, W. D.; Chen, P.; Meyer, T. J. *Inorg. Chem.* **1996**, *35*, 273.
(17) Sung-Suh, H. M.; Kim, D. S.; Lee, C. W.; Park, S. E. *Appl. Organomet. Chem.* **2000**, *14*, 826.
(18) Baranoff, E.; Collin, J.-P.; Furusho, J.; Furusho, Y.; Laemmel, A.-C.; Sauvage, J.-P. *Inorg. Chem.* **2002**, *41*, 1215.
(19) Stoyanov, S. R.; Villegas, J. M.; Rillema, D. P. *Inorg. Chem.* **2002**, *41*, 2941.
(20) Zheng, K. C.; Wang, J. P.; Shen, Y.; Peng, W. L.; Yun, F. C. *J. Chem. Soc., Dalton Trans.* **2002**, 111.
(21) Zheng, K. C.; Wang, J. P.; Peng, W. L.; Shen, Y.; Yun, F. C. *Inorg. Chim. Acta* **2002**, *328*, 247.
(22) Zheng, K.; Wang, J.; Shen, Y.; Peng, W.; Yun, F. *J. Comput. Chem.* **2002**, *23*, 436.
(23) Zheng, K.; Wang, J.; Peng, W.; Liu, X.; Yun, F. *J. Phys. Chem. A* **2001**, *105*, 10899.
(24) Zheng, K.; Wang, J.; Shen, Y.; Kuang, D.; Yun, F. *J. Phys. Chem. A* **2001**, *105*, 7248.
(25) Diaz-Acosta, I.; Baker, J.; Cordes, W.; Pulay, P. *J. Phys. Chem. A* **2001**, *105*, 238.
(26) Dattelbaum, D. M.; Omberg, K. M.; Schoonover, J. R.; Martin, R. L.; Meyer, T. J. *Inorg. Chem.* **2002**, *41*, 6071.
(27) Dattelbaum, D. M.; Martin, R. L.; Schoonover, J. R.; Meyer, T. J. *J. Phys. Chem. A* **2004**, *108*, 3518.
(28) Dattelbaum, D. M.; Omberg, K. M.; Hay, P. J.; Gebhart, N. L.; Martin, R. L.; Schoonover, J. R.; Meyer, T. J. *J. Phys. Chem. A* **2004**, *108*, 3527.
(29) Kleverlaan, C. J.; Stufkens, D. J.; Clark, I. P.; George, M. W.; Turner, J. J.; Martino, D. M.; van Willigen, H.; Vlcek, A. *J. Am. Chem. Soc.* **1998**, *120*, 10871.
(30) Dyer, J.; Blau, W. J.; Coates, C. G.; Creely, C. M.; Gavey, J. D.; George, M. W.; Grills, D. C.; Hudson, S.; Kelly, J. M.; Matousek, P.; McGarvey, J. J.; McMaster, J.; Parker, A. W.; Towrie, M.; Weinstein, J. A. *Photochem. Photobiol. Sci.* **2003**, *2*, 542.
(31) Paur-Afshari, R.; Lin, J.; Schultz, R. H. *Organometallics* **2000**, *19*, 1682.
(32) Baranovic, G.; Babic, D. *Spectrochim. Acta, Part A* **2004**, *60*, 1013.
(33) Ould-Moussa, L.; Castella-Ventura, M.; Kassab, E.; Poizat, O.; Strommen, D. P.; Kincaid, J. R. *J. Raman Spectrosc.* **2000**, *31*, 377.
(34) Bencini, A.; Ciofini, I.; Daul, C. A.; Ferretti, A. *J. Am. Chem. Soc.* **1999**, *121*, 11418.
(35) Sieger, M.; Wanner, M.; Kaim, W.; Stufkens, D. J.; Snoeck, T. L.; Zalis, S. *Inorg. Chem.* **2003**, *42*, 3340.
(36) Uhlmann, V. E.; Thomas, P.; Kempter, G. *Z. Anorg. Allg. Chem.* **1965**, *341*, 11.
(37) Thummel, R.; Lefoulon, F.; Cantu, D.; Mahadevan, R. *J. Org. Chem.* **1984**, *49*, 2208.
(38) Thummel, R. P.; Lefoulon, F. *J. Org. Chem.* **1985**, *50*, 666.
(39) Moya, S. A.; Pastene, R.; Schmidt, R.; Guerrero, J.; Sartori, R. *Polyhedron* **1992**, *11*, 1665.
(40) Junk, T.; Catallo, W. J.; Elguero, J. *Tetrahedron Lett.* **1997**, *38*, 6309.
(41) Microanalyses were obtained using a Carlo Erba EA1108 with TCD detection for H_2O or D_2O.
(42) House, H. O.; Feng, E.; Peet, N. P. *J. Org. Chem.* **1971**, *36*, 2371.
(43) Krejcik, M.; Danek, M.; Hartl, F. *J. Electroanal. Chem.* **1991**, *317*, 179.
(44) Shriver, D. F.; Dunn, J. B. R. *Appl. Spectrosc.* **1974**, *28*, 319.
(45) Frisch, M. J.; Trucks, G. W.; Schlegel, H. B.; Scuseria, G. E.; Robb, M. A.; Cheeseman, J. R.; Montgomery, J. A., Jr.; Vreven, T.; Kudin, K. N.; Burant, J. C.; Millam, J. M.; Iyengar, S. S.; Tomasi, J.; Barone, V.; Mennucci, B.; Cossi, M.; Scalmani, G.; Rega, N.; Petersson, G. A.; Nakatsuji, H.; Hada, M.; Ehara, M.; Toyota, K.; Fukuda, R.; Hasegawa, J.; Ishida, M.; Nakajima, T.; Honda, Y.; Kitao, O.; Nakai, H.; Klene, M.; Li, X.; Knox, J. E.; Hratchian, H. P.; Cross, J. B.; Adamo, C.; Jaramillo, J.; Gomperts, R.; Stratmann, R. E.; Yazyev, O.; Austin, A. J.; Cammi, R.; Pomelli, C.; Ochterski, J. W.; Ayala, P. Y.; Morokuma, K.; Voth, G. A.; Salvador, P.; Dannenberg, J. J.; Zakrzewski, V. G.; Dapprich, S.; Daniels, A. D.; Strain, M. C.; Farkas, O.; Malick, D. K.; Rabuck, A. D.; Raghavachari, K.; Foresman, J. B.; Ortiz, J. V.; Cui, Q.; Baboul, A. G.; Clifford, S.; Cioslowski, J.; Stefanov, B. B.; Liu, G.; Liashenko, A.; Piskorz, P.; Komaromi, I.; Martin, R. L.; Fox, D. J.; Keith, T.; Al-Laham, M. A.; Peng, C. Y.; Nanayakkara, A.; Challacombe, M.; Gill, P. M. W.; Johnson, B.; Chen, W.; Wong, M. W.; Gonzalez, C.; Pople, J. A. *Gaussian 03*; Gaussian, Inc.: Pittsburgh, PA, 2003.
(46) Schaftenaar, G.; Noordik, J. H. *J. Comput.-Aided Mol. Des.* **2000**, *14*, 123.
(47) Portmann, S.; Lüthi, H. P. *Chimia* **2000**, *54*, 766.
(48) Youssef, A. O.; Khalil, M. M. H.; Ramadan, R. M.; Soliman, A. A. *Transition Met. Chem. (Dordrecht, Neth.)* **2003**, *28*, 331.
(49) Bredenbeck, J.; Helbing, J.; Hamm, P. *J. Am. Chem. Soc.* **2004**, *126*, 990.
(50) Morrison, S. L.; Turner, J. J. *J. Mol. Struct.* **1994**, *317*, 39.
(51) The average force constant k_{nr} may be calculated from Stor et al.
(52) Stor, G. J.; Hartl, F.; van Outersterp, J. W. M.; Stufkens, D. J. *Organometallics* **1995**, *14*, 1115.
(53) Polson, M. I. J.; Howell, S. L.; Flood, A.; Blackman, A. G.; Gordon, K. C. *Polyhedron* **2004**, *23*, 1427.
(54) Sherborne, J.; Scott, S. M.; Gordon, K. C. *Inorg. Chim. Acta* **1997**, *260*, 199.
(55) Solomon, E. I., Lever, A. B. P., Eds.; *Inorganic Electronic Structure and Spectroscopy*; John Wiley & Sons: New York, 1999; Vol. II.
(56) Zalis, S.; Farrell, I. R.; Vlcek, A., Jr. *J. Am. Chem. Soc.* **2003**, *125*, 4580.
(57) Czernuszewicz, R. S.; Spiro, T. G. In *Inorganic Electronic Structure and Spectroscopy*; John Wiley & Sons: New York, 1999; Vol. I.
(58) Manuel, D. J.; Strommen, D. P.; Bhuiyan, A.; Sykora, M.; Kincaid, J. R. *J. Raman Spectrosc.* **1997**, *28*, 933.
(59) Flood, A.; Girling, R. B.; Gordon, K. C.; Hester, R. E.; Moore, J. N.; Polson, M. I. J. *J. Raman Spectrosc.* **2002**, *33*, 434.
(60) Clark, R. J. H.; Turtle, P. C.; Strommen, D. P.; Streusand, B.; Kincaid, J. R.; Nakamoto, K. *Inorg. Chem.* **1977**, *16*, 84.
(61) Clark, R. J. H.; Dines, T. J. *Angew. Chem.* **1986**, *98*, 131.
(62) Heller, E. J. *Acc. Chem. Res.* **1981**, *14*, 368.
(63) Shin, K. S.; Clark, R. J. H.; Zink, J. I. *J. Am. Chem. Soc.* **1989**, *111*, 4244.
(64) Waterland, M. R.; Gordon, K. C.; McGarvey, J. J.; Jayaweera, P. M. *J. Chem. Soc., Dalton Trans.* **1998**, 609.
(65) Waterland, M. R.; Simpson, T. J.; Gordon, K. C.; Burrell, A. K. *J. Chem. Soc., Dalton Trans.* **1998**, 185.
(66) The donor orbital in the MLCT transition is responsible for the enhancement of the CO vibration.
(67) Kato, T.; Shida, T. *J. Am. Chem. Soc.* **1979**, *101*, 6869.
(68) Hiratsuka, H.; Sekiguchi, K.; Hatano, Y.; Tanizaki, Y.; Mori, Y. *Can. J. Chem.* **1987**, *65*, 1185.
(69) Schoonover, J. R.; Gordon, K. C.; Argazzi, R.; Woodruff, W. H.; Peterson, K. A.; Bignozzi, C. A.; Dyer, R. B.; Meyer, T. J. *J. Am. Chem. Soc.* **1993**, *115*, 10996.
(70) Stufkens, D. J.; Vlcek, A., Jr. *Coord. Chem. Rev.* **1998**, *177*, 127.
(71) Stufkens, D. J. *Comments Inorg. Chem.* **1992**, *13*, 359.
(72) Schoonover, J. R.; Chen, P.; Bates, W. D.; Dyer, R. B.; Meyer, T. J. *Inorg. Chem.* **1994**, *33*, 793.
(73) Kaim, W.; Kohlmann, S. *Inorg. Chem.* **1990**, *29*, 2909.